applied sciences

MDPI

Article

Establishment and Accuracy Analysis of Measurement Control Network Based on Length–Angle Mixed Intersection Adjustment Model

Zhi Xiong [1,2,*], Chunsen Li [1,2], Hao Zhang [1,2], Chenxiaopeng Zhong [1,2], Zhongsheng Zhai [1,2] and Ziyue Zhao [3]

[1] School of Mechanical Engineering, Hubei University of Technology, Wuhan 430068, China; 102100051@hbut.edu.cn (C.L.); zh205779@163.com (H.Z.); zhongcxp@163.com (C.Z.); zs.zhai@hbut.edu.cn (Z.Z.)
[2] Hubei Key Laboratory of Modern Manufacture Quality Engineering, Wuhan 430068, China
[3] AVIC Beijing Changcheng Institute of Metrology & Measurement, Beijing 100095, China; 18500366376@163.com
* Correspondence: xiongzhi0611@163.com

Abstract: To achieve high-precision measurements of target points on long straight tracks, a multi-level measurement method based on length–angle mixed intersection techniques was explored. Firstly, a control network with graded measurement levels was proposed, based on the spatial error characteristics of different measuring devices and the principle of nonlinear least squares, and a method for adjustment calculation based on length–angle mixed intersection was studied. Secondly, numerical simulation was conducted to assess the impact of instrument placement on measurement accuracy, and the results indicated that central positioning within the measurement range can effectively minimize the overall point location errors. Finally, the methodology was validated in a practical setting at a rocket sled test site. Experimental results demonstrated that, within a measurement range of approximately 669 m, when target points were located on one side of the track and distance measurements were used as benchmark values, the measurement control network achieved a distance standard deviation of 0.20 mm. The range of distance deviations was between −0.85 mm and 0.98 mm. This approach offers substantial reference value for high-precision coordinate measurements over extended distances.

Keywords: measurement control network; graded measurement; length–angle mixed intersection; layout simulation

check for updates

Citation: Xiong, Z.; Li, C.; Zhang, H.; Zhong, C.; Zhai, Z.; Zhao, Z. Establishment and Accuracy Analysis of Measurement Control Network Based on Length–Angle Mixed Intersection Adjustment Model. *Appl. Sci.* **2024**, *14*, 4948. https://doi.org/10.3390/app14114948

Academic Editor: Luca Poletto

Received: 17 April 2024
Revised: 4 June 2024
Accepted: 5 June 2024
Published: 6 June 2024

Copyright: © 2024 by the authors. Licensee MDPI, Basel, Switzerland. This article is an open access article distributed under the terms and conditions of the Creative Commons Attribution (CC BY) license (https://creativecommons.org/licenses/by/4.0/).

1. Introduction

Modern large-scale precision coordinate measurement technology is an interdisciplinary subject that encompasses electronics, optics, sensors, and computer technology. It is extensively applied in the industrial measurement fields of large-scale equipment manufacturing such as aircraft assembly, particle accelerators, and rocket sled tests [1]. During aircraft assembly, it is essential to unify components under a high-precision three-dimensional coordinate measurement control network for real-time monitoring and correction of overall accuracy. Particle accelerators consist of thousands of complex and precision components, the installation of which demands rigorous precision measurement techniques and methods for global accuracy control. In rocket sled tests, the sled's speed and acceleration are indirectly measured through the measurement of positional coordinates along one side of the track, which establishes a high-precision three-dimensional control network that plays a crucial role in evaluating the performance of inertial navigation systems. Additionally, large-scale precision coordinate measurement holds promising prospects for application in engineering measurement involving high-rise buildings and transportation infrastructure over long distances. With the advancement of technology and the requirements of

large-scale engineering measurement, large-scale coordinate measurement systems are increasingly utilized in the precision positioning, collimation measurements, adjustment assembly, installation maintenance, and structural verification of large equipment [2].

Due to the limited measuring range of a single measurement device, as the working distance increases, the measurement error of a single measurement device also increases, highlighting the contradiction between range and precision [3–6]. For large-scale coordinate measurement schemes, a network measurement approach using multiple devices is often adopted. The Unified Spatial Metrology Network (USMN) technology [7] has gradually developed, primarily to solve the network adjustment problems of various spherical coordinate measurement systems (such as laser trackers, total stations, and laser theodolites). Muelaner has formed a distributed coordinate measurement system, the indoor GPS system, in a 10 m × 10 m × 1.5 m measurement space, with a coordinate measurement uncertainty of about ±1 mm at a 95% confidence level [8]. Although the precision of the iGPS system is not affected by the measuring range, the system is not suitable for outdoor measurements and requires certain environmental conditions. The larger the measurement range, the more devices are needed for networking, thus increasing the cost. Manwiller used a laser tracker to establish a three-dimensional control network in FRIB tunnel, which is approximately 170 m in length. In the tunnel, 30 station positions were set to measure 306 target points, achieving one sigma value each in the x, y, and z directions of 16 μm, 26 μm, and 34 μm, respectively, after adjustment [9]. Xing et al. proposed a method to establish a control network for accelerator tunnels using total station angle observations and the high-precision ranging values of the laser tracker, completing the measurement in a 230 m circular accelerator using an angle intersection measurement method and achieving an overall planar accuracy of 66 μm [10]. Guillory et al. used a total station and a multilateral measurement system to build a global measurement network, completing the measurement tasks at the Geodetic Observatory Wettzell, within a range of 73 m. The standard deviations of the reference points in the x, y, and z directions were 0.06 mm, 0.04 mm, and 0.10 mm, respectively [11]. The above studies achieved target point coordinate measurements in a range of about 200 m, and the results show that the larger the measurement range, the lower the coordinate measurement precision, and when the measurement range is further expanded, such as to 500 m or even longer distances, the methods mentioned in these references cannot be directly applied. Therefore, a new coordinate measurement method for even longer distances is studied in this article.

In addition, the coordinate system conversion between multiple stations is involved in the measurement process of multiple device networking [12], so the layout of devices [13] and their common points among affect the measurement precision. Sheng et al. used an improved genetic algorithm (GA) to optimize the layout of multiple laser trackers [14]. Yang et al. arranged laser tracker stations at different heights in the center of a circular plane, which improved the coordinate measurement accuracy [15]. Shang et al., through simulation analysis, found that when four laser trackers form a right-angle regular triangular pyramid, the highest coordinate measurement accuracy can be obtained [16]. The above studies show that layout optimization provides theoretical guidance for practical networking, which can save measurement time, improve measurement efficiency, and even reduce costs. Therefore, based on the research of coordinate measurement method, the simulation analysis of the layout optimization of measurement devices is also conducted in this article.

This article proposes a multi-level measurement method based on multi-type devices suitable for ultra-long distances, taking the target point coordinates on a rocket sled test track as the measurement object. A series of valuable conclusions are obtained through simulations and experiments. And the main contributions in this article are summarized as follows:

- The measurement control network is graded, and a multi-level measurement and step-by-step control model was designed, providing a guarantee for overall measurement accuracy.

- A length–angle mixed intersection adjustment model was established. Mathematical expressions for the projection of horizontal angles in different quadrants were derived to ensure the accuracy of model solutions. The model is applicable not only to the same devices but also to the different types of equipment.
- Simulation analysis of the layout of measurement instruments was conducted, providing guidance for the setup of the measurement control network.
- The method presented in this article has significant reference value for the construction of straight-track measurement networks and can be applied in large-scale projects such as power plant construction, tunnel construction, and oil and gas pipeline construction.

In the rest of this article, Section 2 describes the establishment of the measurement control network. Section 3 describes the simulation analysis of the layout of measurement equipment and the adjustment model. Section 4 presents experimental results and analysis. Finally, Section 5 concludes the article.

2. Establishment of Measurement Control Network Model

2.1. Description of Measurement Control Network Grading

Considering the vast distribution and numerous target points along long-distance tracks, using a single measurement device is insufficient to measure all target points and ensure the accuracy requirements. The total station offers a large measurement range, but it tends to have relatively large measurement errors at shorter distances, whereas the laser tracker provides high precision but has a limited maximum measuring range. Segmental measurement approaches using the laser tracker could lead to significant cumulative errors, failing to meet the full-range measurement requirements. Therefore, laser tracker and total station are used to establish a measurement control network, adopting a multi-level measurement and step-by-step control strategy to achieve high-precision coordinate measurement of target points on long-distance tracks.

As shown in Figure 1, the measurement control network is divided into several levels: Level I corresponds to the distance between each of the two adjacent target points; Level II and higher levels are defined based on the characteristics of the measuring device. This multi-level measurement is defined as a network grading model. For example, with a total distance of 500 m, a laser tracker could be chosen as the measuring instrument within Level II and the total station as the measuring instrument within Level III. The key to ensuring measurement precision lies in how the data from Level II and Level III are integrated and transformed into the global coordinate system.

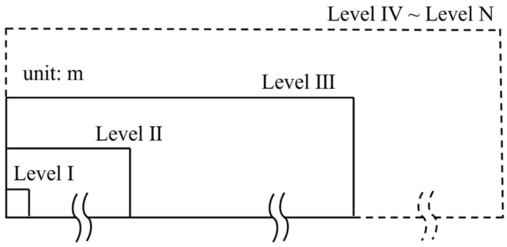


Figure 1. Grading of measurement control network.

2.2. Error Characteristics Analysis of Measuring Instruments

The horizontal and vertical angle encoders of laser tracker and total station provide azimuth angle α and zenith angle β relative to their own center spheroid coordinate system. D is the return oblique distance. The schematic diagram of the coordinate system for such devices is shown in Figure 2. By projecting Point (X, Y, Z) onto the xoy and yoz planes,

respectively, the conversion relationship from spherical coordinates to cartesian coordinates can be obtained as follows:

$$\begin{cases} X &= D{\cdot}cos\alpha{\cdot}sin\beta \\ Y &= D{\cdot}sin\alpha{\cdot}sin\beta \\ Z &= D{\cdot}cos\beta \end{cases} \quad (1)$$

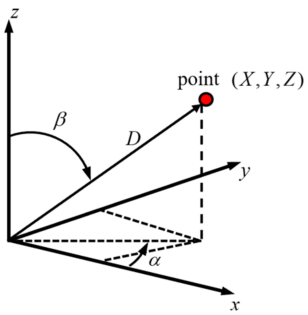


Figure 2. Schematic of the coordinate system of the measuring instrument.

Taking the Leica AT402 absolute laser tracker as an example, the device offers a measurement range from 1.5 m to 80 m, a vertical range of ±45°. It employs ADM technology to perform absolute distance measurement and has a constant error of ±10 μm in distance measurement, as well as an angular measurement accuracy of ±(15 μm + 6 μm/m). As depicted in Figure 3, angular measurement error decreases as the measurement distance increases, and finally stabilizes to about 1.28″, which is inversely proportional to the measured distance.

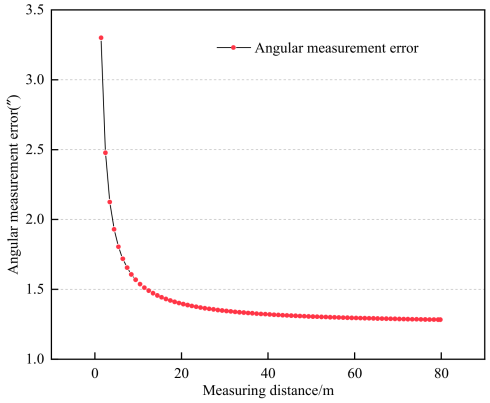
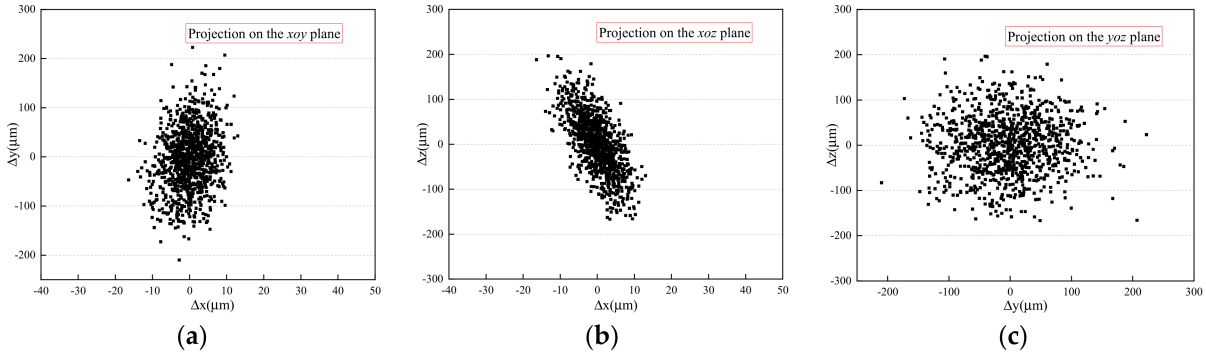


Figure 3. Angular measurement error of the laser tracker.

A point at (−30,000, 500, −1500) mm is chosen to be repeatedly observed 1000 times using the laser tracker, and the repeatability cloud is produced. Figure 4a–c displays the projections of the three-dimensional repeatability cloud on the xoz, xoy, and yoz planes, respectively. The coordinate measurement errors of the laser tracker are greater in the y and z directions, indicating that errors in the horizontal direction are smaller than those in the vertical direction. The repeatability cloud projected on the xoz and xoy plane is upward at an angle, forming an elliptical distribution; on the yoz planes, the projections appear as irregular circular distributions.

Simulation analysis confirms that, within an effective measuring range, the laser tracker can achieve a single-point coordinate measurement accuracy better than 266 μm. However, due to the limited range of the laser tracker, using it alone to measure target points across an entire range necessitates multiple station transfers, leading to error accumulation.



(**a**) (**b**) (**c**)

Figure 4. Repeatability cloud for single−point coordinate measurement by laser tracker: (**a**) projection on the xoy plane; (**b**) projection on the xoz plane; and (**c**) projection on the yoz plane.

Moreover, an error analysis is performed using the Leica MS60 total station as an example, which offers angular measurement precision of 0.5″, distance measurement range extends from 1.5 m to more than 10,000 m with a prism and from 1.5 m to 2000 m without a prism with a distance measurement accuracy of 1.2 mm + 2 mm/km. The total station performs repeated observations on a point at (−15,000, 2500, −2500) mm in space, resulting in the repeatability cloud as shown in Figure 5. The analysis shows that the total station's measurement errors mainly concentrate longitudinally along the x and y directions. As shown in Figure 6a–c, measurement errors predominantly occur in the x direction, with significantly smaller errors in the y and z directions.

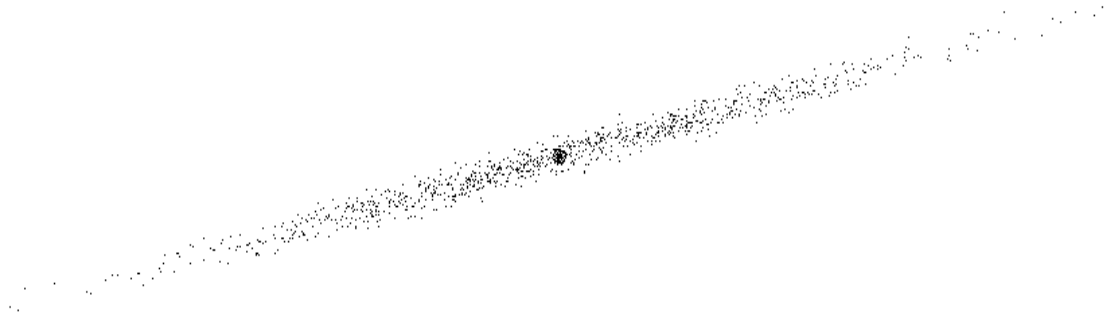
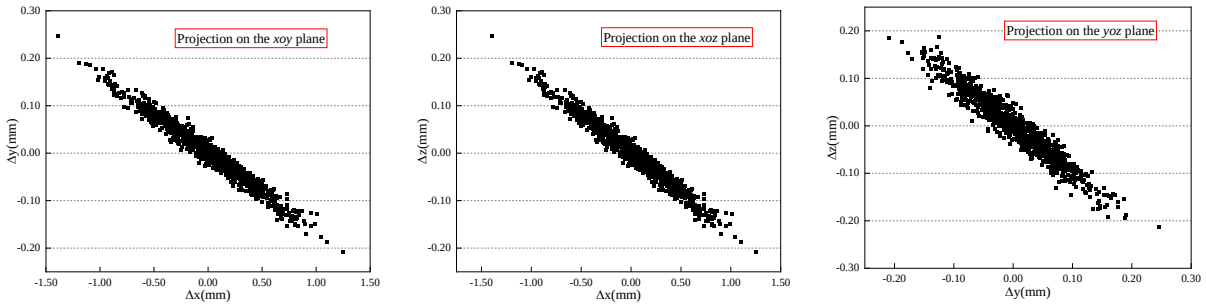


Figure 5. Repeatability cloud for single−point coordinate measurement by total station.



(**a**) (**b**) (**c**)

Figure 6. Repeatability cloud of single−point measurement error in the x, y, and z directions by total station: (**a**) projection on the xoy plane; (**b**) projection on the xoz plane; and (**c**) projection on the yoz plane.

From the above simulation analysis, it is evident that the total station's extensive measurement range and high angular precision significantly compensate for the limitations of the laser tracker. Using a total station to repeatedly measure the simulated point, the maximum error in single-point coordinate measurement within a range of 15 m can reach

1.43 mm, which indicates that using only the total station is unsuitable for measuring target points across the large range.

In summary, the laser tracker has a limited measuring range but high coordinate measurement accuracy, particularly the interferometric distance measurement precision, which can reach the ppm level. The total station, on the other hand, offers a larger measuring range and lower coordinate measurement accuracy, but its high angular measurement precision should not be overlooked. How to utilize the high distance measurement precision of the laser tracker and the high angular measurement precision of the total station within a large-scale measurement range is one of the key research aims of this article.

2.3. Length–Angle Mixed Intersection Adjustment Method

Based on the error characteristics analysis of the laser tracker and total station described above, an adjustment method based on length–angle mixed intersection is established. As shown in Figure 7, the track orientation is defined as the x-axis direction, with the direction perpendicular to the track defined as the y-axis direction. Target points are placed equidistantly along the x-axis on one side of the track, consisting of fixed base and target ball. The target ball is a spherical reflector.

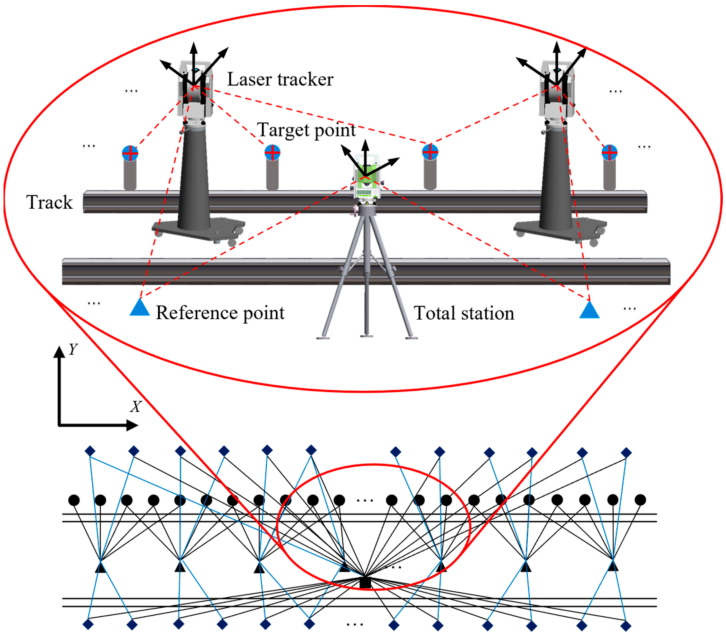


Figure 7. Distribution of target points, reference points, and stations on a long track.

To establish a linkage between the total station (Level III) and the laser tracker (Level II), reference points are deployed around the track, which consist of movable base and target ball, and the target ball is a spherical reflector. The laser tracker performs coordinate measurements of both target and reference points within its measuring range, while the total station conducts the coordinate measurements of reference points within its range.

For the construction of a measuring network for target and reference points depicted in Figure 7, we assume that m measuring stations are set up inside the track with the laser tracker and total station measurement systems. These systems observe distances and angles of n measuring points. The length and angle observation from the ith measuring station to the jth point is denoted as $(D_{ij}, \alpha_{ij}, \beta_{ij})$, with the spatial position parameters of the station's center being (t_{xi}, t_{yi}, t_{zi}) $(i = 1, 2, \ldots, m)$. The coordinates of the jth measuring point in the coordinate system (local coordinate system) of the ith measuring station are represented as (X_{ij}, Y_{ij}, Z_{ij}) $(j = 1, 2, \ldots, n)$, and in the global coordinate system, as (X_j, Y_j, Z_j). Defining the coordinate system of the total station as the global coordinate system, the rotation matrix $\boldsymbol{R}_i$ and translation vector $\boldsymbol{T}_i$ relative to the global coordinate system for the other measuring

stations' coordinate systems are obtained through a common point transformation model. The relationship between (X_j, Y_j, Z_j) and (X_{ij}, Y_{ij}, Z_{ij}) is expressed as follows:

$$\begin{pmatrix} X_j \\ Y_j \\ Z_j \end{pmatrix} = \boldsymbol{R}_i \times \begin{pmatrix} X_{ij} \\ Y_{ij} \\ Z_{ij} \end{pmatrix} + \boldsymbol{T}_i \tag{2}$$

In the formula, $\boldsymbol{T}_i = (t_{xi}, t_{yi}, t_{zi})^T$, $\boldsymbol{R}_i = \boldsymbol{R}y_i \times \boldsymbol{R}x_i \times \boldsymbol{R}z_i$ ($\boldsymbol{R}x_i$, $\boldsymbol{R}y_i$, $\boldsymbol{R}z_i$ are the rotation matrices for the x, y, and z axes, respectively).

As can be seen from Formula (1), the functional relationship between the coordinates of the measuring points at the ith station and the horizontal and zenith angles are as follows:

$$\alpha_{ij} = \begin{cases} arctan\frac{Y_{ij}}{X_{ij}}, & X_{ij} > 0 \\ \pi + arctan\frac{Y_{ij}}{X_{ij}}, & X_{ij} < 0, Y_{ij} > 0 \\ -\pi + arctan\frac{Y_{ij}}{X_{ij}}, & X_{ij} < 0, Y_{ij} < 0 \end{cases} \tag{3}$$

$$\beta_{ij} = \frac{\pi}{2} - arctan\frac{Z_{ij}}{\sqrt{X_{ij}^2 + Y_{ij}^2}} \tag{4}$$

The coordinates of the measuring points in the above two equations are expressed in the local coordinate system. Using Formula (2) to convert them to the global coordinate system, Formula (4) is expressed as follows:

$$\beta_{ij}^0 = \frac{\pi}{2} - arctan\frac{Z_j - t_{zi}}{\sqrt{(X_j - t_{xi})^2 + (Y_j - t_{yi})^2}} \tag{5}$$

The relationship between the coordinates of points and distance observations in the global coordinate system is as follows:

$$D_{ij}^0 = \sqrt{(X_j - t_{xi})^2 + (Y_j - t_{yi})^2 + (Z_j - t_{zi})^2} \tag{6}$$

Due to the rotation of the coordinate systems, there is an angle between the O-X axis of the global coordinate system O_1-X_1 Y_1 Z_1 and the local coordinate system O_i-X_i Y_i Z_i (i = 2, . . ., m) as shown in Figure 8.

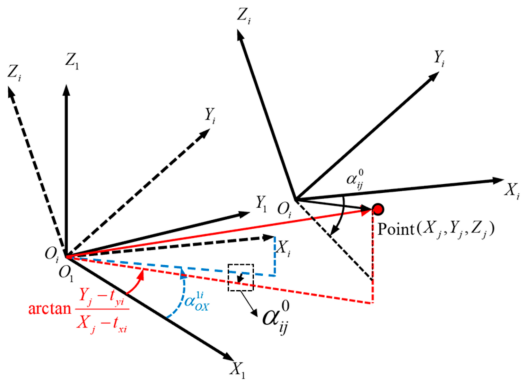


Figure 8. The schematic diagram for calculating the horizontal angle α in the global coordinate system.

Therefore, when calculating the horizontal angle using the transformed global coordinates of the measurement points, it is necessary to consider not only the angle and direction between the x axes but also which quadrant the projection of vector $\overrightarrow{\boldsymbol{O_1P}}$ falls onto. The

calculation formula for the horizontal angle α_{ij}^0 in the global coordinate system should be divided into four cases:

(1) when vector $\overrightarrow{O_1P}$ projects onto the first quadrant,

$$\alpha_{ij}^0 = \begin{cases} arctan\frac{Y_j - t_{yi}}{X_j - t_{xi}} - \alpha_{OX}^{1i}, \alpha_{OX}^{1i} > \alpha_0 - \pi \\ -2\pi + arctan\frac{Y_j - t_{yi}}{X_j - t_{xi}} - \alpha_{OX}^{1i}, \alpha_{OX}^{1i} \in [-2\pi, -\frac{\pi}{2}] \cup \alpha_{OX}^{1i} < \alpha_0 - \pi \end{cases} \tag{7}$$

(2) when vector $\overrightarrow{O_1P}$ projects onto the second quadrant,

$$\alpha_{ij}^0 = \begin{cases} \pi + arctan\frac{Y_j - t_{yi}}{X_j - t_{xi}} - \alpha_{OX}^{1i}, \alpha_{OX}^{1i} \notin (-2\pi, -\frac{\pi}{2}) \cup \alpha_{OX}^{1i} > \alpha_0 \\ -\pi + arctan\frac{Y_j - t_{yi}}{X_j - t_{xi}} - \alpha_{OX}^{1i}, \alpha_{OX}^{1i} < \alpha_0 \end{cases} \tag{8}$$

(3) when vector $\overrightarrow{O_1P}$ projects onto the third quadrant,

$$\alpha_{ij}^0 = \begin{cases} \pi + arctan\frac{Y_j - t_{yi}}{X_j - t_{xi}} - \alpha_{OX}^{1i}, \alpha_{OX}^{1i} \in [max(\frac{\pi}{2}, \alpha_0), 2\pi] \\ -\pi + arctan\frac{Y_j - t_{yi}}{X_j - t_{xi}} - \alpha_{OX}^{1i}, \alpha_{OX}^{1i} \in (-\frac{\pi}{2}, min(0, \alpha_0)] \end{cases} \tag{9}$$

(4) when vector $\overrightarrow{O_1P}$ projects onto the fourth quadrant,

$$\alpha_{ij}^0 = \begin{cases} arctan\frac{Y_j - t_{yi}}{X_j - t_{xi}} - \alpha_{OX}^{1i}, \alpha_{OX}^{1i} < \alpha_0 + \pi \\ 2\pi + arctan\frac{Y_j - t_{yi}}{X_j - t_{xi}} - \alpha_{OX}^{1i}, \alpha_{OX}^{1i} > \alpha_0 + \pi \end{cases} \tag{10}$$

where $\alpha_0 = arctan\frac{Y_j - t_{yi}}{X_j - t_{xi}}$, α_{OX}^{1i} represents the angle between the x axis of the global coordinate system and the local coordinate system.

The general form of the equations for calculating distances and angles in the global coordinate system are as follows:

$$\begin{cases} D_{ij}^0 = F_{ij}^D(t_{x1}, t_{y1}, t_{z1}, \ldots, t_{xi}, t_{yi}, t_{zi}, X_1, Y_1, Z_1, \ldots, X_j, Y_j, Z_j) \\ \alpha_{ij}^0 = F_{ij}^\alpha(t_{x1}, t_{y1}, t_{z1}, \ldots, t_{xi}, t_{yi}, t_{zi}, X_1, Y_1, Z_1, \ldots, X_j, Y_j, Z_j) \\ \beta_{ij}^0 = F_{ij}^\beta(t_{x1}, t_{y1}, t_{z1}, \ldots, t_{xi}, t_{yi}, t_{zi}, X_1, Y_1, Z_1, , \ldots, X_j, Y_j, Z_j) \end{cases} \tag{11}$$

Since Formula (11) is a nonlinear function, it is necessary to linearize the observation equation. Linearization of the observation equation generally involves using the Taylor series expansion, taking the first-order term and omitting terms of second order and higher. By setting $\delta \boldsymbol{x} = \boldsymbol{x} - \boldsymbol{x}^0$, the linearized form of Formula (11) is presented as follows:

$$\begin{cases} D_{ij} + \Delta_{ij}^D = F_{ij}^{D^0} + \left.\frac{\partial F_{ij}^D}{\partial t_{xi}}\right|_{x^0} \cdot \delta t_{xi} + \left.\frac{\partial F_{ij}^D}{\partial t_{yi}}\right|_{x^0} \cdot \delta t_{yi} + \left.\frac{\partial F_{ij}^D}{\partial t_{zi}}\right|_{x^0} \cdot \delta t_{zi} + \left.\frac{\partial F_{ij}^D}{\partial X_j}\right|_{x^0} \cdot \delta X_j + \left.\frac{\partial F_{ij}^D}{\partial Y_j}\right|_{x^0} \cdot \delta Y_j + \left.\frac{\partial F_{ij}^D}{\partial Z_j}\right|_{x^0} \cdot \delta Z_j \\ \alpha_{ij} + \Delta_{ij}^\alpha = F_{ij}^{\alpha 0} + \left.\frac{\partial F_{ij}^\alpha}{\partial t_{xi}}\right|_{x^0} \cdot \delta t_{xi} + \left.\frac{\partial F_{ij}^\alpha}{\partial t_{yi}}\right|_{x^0} \cdot \delta t_{yi} + \left.\frac{\partial F_{ij}^\alpha}{\partial t_{zi}}\right|_{x^0} \cdot \delta t_{zi} + \left.\frac{\partial F_{ij}^\alpha}{\partial X_j}\right|_{x^0} \cdot \delta X_j + \left.\frac{\partial F_{ij}^\alpha}{\partial Y_j}\right|_{x^0} \cdot \delta Y_j + \left.\frac{\partial F_{ij}^\alpha}{\partial Z_j}\right|_{x^0} \cdot \delta Z_j \\ \beta_{ij} + \Delta_{ij}^\beta = F_{ij}^{\beta 0} + \left.\frac{\partial F_{ij}^\beta}{\partial t_{xi}}\right|_{x^0} \cdot \delta t_{xi} + \left.\frac{\partial F_{ij}^\beta}{\partial t_{yi}}\right|_{x^0} \cdot \delta t_{yi} + \left.\frac{\partial F_{ij}^\beta}{\partial t_{zi}}\right|_{x^0} \cdot \delta t_{zi} + \left.\frac{\partial F_{ij}^\beta}{\partial X_j}\right|_{x^0} \cdot \delta X_j + \left.\frac{\partial F_{ij}^\beta}{\partial Y_j}\right|_{x^0} \cdot \delta Y_j + \left.\frac{\partial F_{ij}^\beta}{\partial Z_j}\right|_{x^0} \cdot \delta Z_j \end{cases} \tag{12}$$

For the adjustment model of mixed intersection of lengths and angles, the error matrix equation is constructed according to the following principles:

(1) Total station observes the reference points, and only the angle observations of the reference points are retained when the observation error equation is established.

(2) Laser tracker observes the target points and reference points. When presenting the error equations for the observations, all observations of target points are retained, and only the distance observations of reference points are retained.

Then, Formula (9) can be expressed in the matrix form:

$$\Delta = \boldsymbol{A} \cdot \delta \boldsymbol{x} - (\boldsymbol{L} - \boldsymbol{d}) \tag{13}$$

where $\Delta = \left(\Delta_{ij}^{D}, \Delta_{ij}^{\alpha}, \Delta_{ij}^{\beta}\right)^{T}$ is the residual vector; $\boldsymbol{d} = \left(\boldsymbol{F}_{ij}^{D0}, \boldsymbol{F}_{ij}^{\alpha 0}, \boldsymbol{F}_{ij}^{\beta 0}\right)^{T}$ is the initial value of observations; $\boldsymbol{L} = \left(D_{ij}, \alpha_{ij}, \beta_{ij}\right)^{T}$ contains the angle observation information of reference points by the total station, with all observation information of the laser tracker on target points and distance observation information of reference points; $\boldsymbol{A}$ is the coefficient matrix of the error equation, as follows in Formula (14):

$$\boldsymbol{A}_{3mn\times 3(m+n)} = \begin{pmatrix} \frac{\partial F_{ij}^{D}}{\partial t_{x1}} & \frac{\partial F_{ij}^{D}}{\partial t_{y1}} & \frac{\partial F_{ij}^{D}}{\partial t_{z1}} & \cdots & \frac{\partial F_{ij}^{D}}{\partial X_{1}} & \frac{\partial F_{ij}^{D}}{\partial Y_{1}} & \frac{\partial F_{ij}^{D}}{\partial Z_{1}} & \cdots \\ \vdots & \vdots & \vdots & \ddots & \vdots & \vdots & \vdots & \ddots \\ \frac{\partial F_{ij}^{\alpha}}{\partial t_{xi}} & \frac{\partial F_{ij}^{\alpha}}{\partial t_{yi}} & \frac{\partial F_{ij}^{\alpha}}{\partial t_{zi}} & \cdots & \frac{\partial F_{ij}^{\alpha}}{\partial X_{j}} & \frac{\partial F_{ij}^{\alpha}}{\partial Y_{j}} & \frac{\partial F_{ij}^{\alpha}}{\partial Z_{j}} & \cdots \\ \vdots & \vdots & \vdots & \ddots & \vdots & \vdots & \vdots & \ddots \\ \frac{\partial F_{ij}^{\beta}}{\partial t_{xi}} & \frac{\partial F_{ij}^{\beta}}{\partial t_{yi}} & \frac{\partial F_{ij}^{\beta}}{\partial t_{zi}} & \cdots & \frac{\partial F_{ij}^{\beta}}{\partial X_{j}} & \frac{\partial F_{ij}^{\beta}}{\partial Y_{j}} & \frac{\partial F_{ij}^{\beta}}{\partial Z_{j}} & \cdots \end{pmatrix} \tag{14}$$

Assuming that there are m_1 laser trackers and m_2 total stations among m measuring stations, there are n_1 target points and n_2 reference points among the n measurement points. Without considering the rotation parameters of measuring stations, the number of unknowns U and the number of equations E in Formula (13) are as follows:

$$\begin{cases} U = 3(m-1) + 3n \\ E = 3m_1n_1 + m_1n_2 + 2m_2n_2 \end{cases} \tag{15}$$

Considering that the condition for the equation to have a solution is that the number of equations is greater than the number of unknowns, that is, $E \geq U$, for the sake of convenient calculation, setting $m_2 = 1$, then the condition is as follows:

$$m_1 \geq 1 + \frac{3n_1 + 2n_2}{n_1 - n_2 - 3} \tag{16}$$

In the formula, m_1, n_1, and n_2 are positive integers, and $n_2 \neq 0$. The condition for Formula (13) to have a solution is to satisfy Formula (16).

The calculation of Formula (13) according to the least squares principle leads to the solution of the unknown parameter as follows:

$$\delta \boldsymbol{x} = \left(\boldsymbol{A}^{T}\boldsymbol{P}\boldsymbol{A}\right)^{-1} \cdot \boldsymbol{A}^{T}\boldsymbol{P} \cdot (\boldsymbol{L} - \boldsymbol{d}) \tag{17}$$

where $\boldsymbol{P}$ is observation weight matrix.

3. Simulation Analysis

3.1. Analysis of Influence of the Layout of Instruments within Level II

The accuracy of the length–angle mixed intersection adjustment model is affected by many factors, mainly including the layout of stations and the distribution of target points.

Assuming that laser trackers are set at different locations within the 72 m measuring range, as shown in Figure 9, where position I is at the edge of the measuring range and position IV is in the middle, the coordinates of target points are observed. The average measurement errors of the laser tracker at positions I through IV for all target points are 0.33 mm, 0.25 mm, 0.20 mm, and 0.18 mm, respectively, as shown in Figure 10. The analysis

shows that, due to the particularity of the laser tracker measurement system, the distance of the measuring distance directly affects the measurement accuracy. Therefore, in the actual measurement, the instrument is generally set in the middle of the measurement range, the measurement error of the overall position coordinates can be minimized, the error of the initial value in the adjustment model can be also further reduced, and the accuracy of the model solution can be improved.

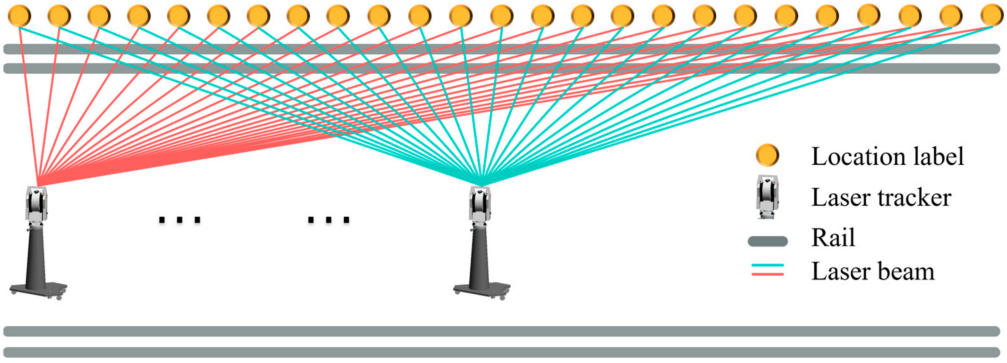


Figure 9. The schematic diagram of measuring station distribution.

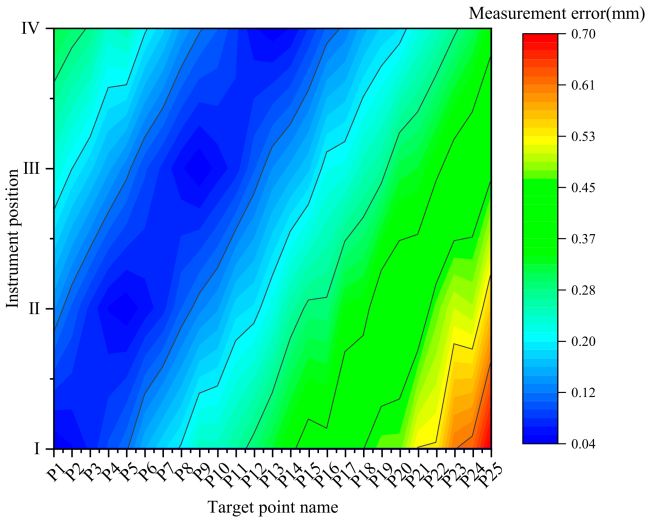


Figure 10. Contour plot of measurement error of target point coordinates under different instrument positions.

3.2. Simulation of Adjustment Algorithm

Based on the optimal locations simulated in Section 3.1 and the length–angle mixed intersection adjustment method proposed in this paper, simulation analysis was conducted using MATLAB to estimate the measurement performance of this method within a range of 660 m. The simulation conditions are as follows: the track length is set to 660 m, with target points placed every 3 m along one side of the track, totaling 221 target points; overall, 44 reference points are distributed around the track, and 11 laser trackers are mounted along the track's centerline and positioned in the middle of the measurement range as illustrated in Figure 10, with the instruments at a height of 1.5 m from the track and two meters away from the target points. The total station and the laser trackers are on the same horizontal plane, with the total station positioned in the middle of the measurement range, and the total station is one meter away from the laser tracker along the y axis, measuring reference points along the long track. The measurement accuracy of the laser tracker and the total station is consistent with that described in Section 2.2.

The measurement of the above target point and reference point is repeated 1000 times. The measurement results of each time are substituted into the adjustment model to obtain the coordinate correction value $\delta x = (\delta \boldsymbol{X}_1, \delta \boldsymbol{Y}_1, \delta \boldsymbol{Z}_1, \ldots, \delta \mathbf{X}_{n_1}, \delta \boldsymbol{Y}_{n_1}, \delta \boldsymbol{Z}_{n_1})^T$ of the target point. Taking the X-direction of the target point coordinates as an example, the standard deviation formula is defined as follows:

$$\begin{cases} \Delta X_k = [X_{n_1} + \delta X_{n_1} - x_{n_1}]_{k \times 1} \\ \sigma_{X_{n_1}} = \sqrt{\frac{\sum_{k=1}^{M} (\Delta X_k)^2}{M-1}} \end{cases} \tag{18}$$

In this formula, $\Delta \boldsymbol{X}_k$ represents the difference between the adjusted value and the theoretical value of the X-direction coordinate of target points after repeating measurements M times, and $\sigma_{X_{n_1}}$ represents the standard deviation of the X-direction coordinate of target points after repeating measurements M times. The composite standard deviation of the target points in three directions can be determined according to Formula (19):

$$\sigma_{P_{n_1}} = \sqrt{{\sigma_{X_{n_1}}}^2 + {\sigma_{Y_{n_1}}}^2 + {\sigma_{Z_{n_1}}}^2} \tag{19}$$

Simulation results based on the principle of nonlinear least squares are obtained in Figure 11, which indicate that the standard deviation of target points can be controlled to below 3.42 mm after adjustment over a measurement distance of 660 m. Throughout the entire long track, target points' standard deviation is significantly influenced by standard deviation in the y and z directions, with X-direction standard deviation being less than 0.29 mm. The total station is positioned at 330 m, and the positional standard deviation for target points that is closer to it is smaller.

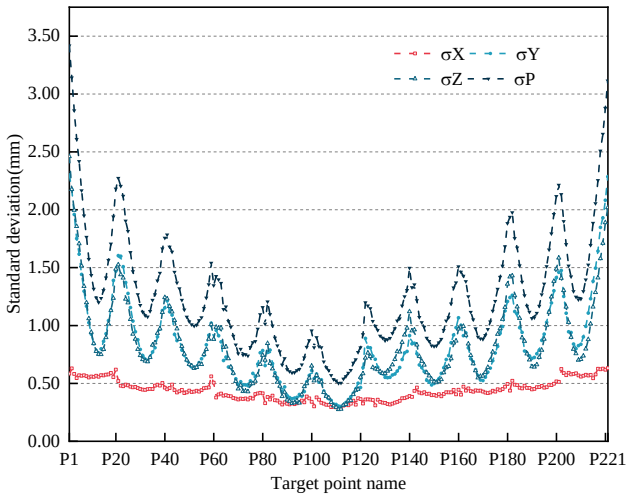


Figure 11. Standard deviation of target points after adjustment.

Based on the above simulation conditions, we set the coordinate system of the sixth laser tracker station as the global coordinate system and remove the total station. Through the continuous station transfers of two adjacent trackers, the target point in the global coordinate system is obtained. The simulation results indicate that, when only laser trackers are used to establish control measurement network, the standard deviation is larger in long-distance measurement ranges compared to the length–angle mixed intersection adjustment model, as shown in Figure 12. Due to multiple station transfers, error propagation and accumulation occur, resulting in larger errors for target points near the global station in the diagram.

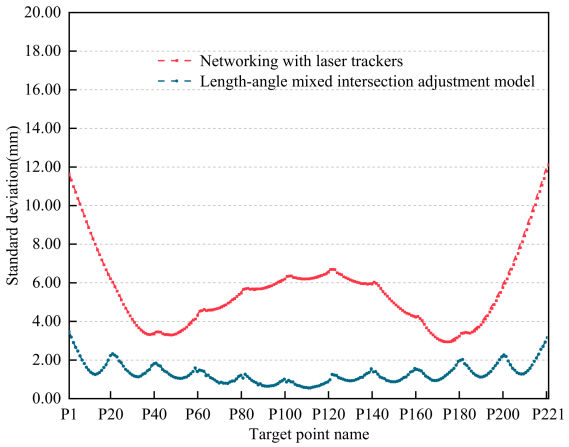


Figure 12. Standard deviation of target points after adjustment compared to networking with laser trackers.

4. Experimental Validation

4.1. Introduction of the Experiment

To validate the applicability and feasibility of the length–angle mixed intersection adjustment method presented in this article, an experimental test is conducted on a section of track at a rocket sled test site. The experimental flow is shown in Figure 13, and the specific experimental steps are as follows:

1. Verify the repeatability of the distance measurement of the tracking instrument;
2. Place the total station in the global position and the laser tracker at L1;
3. Measure the reference points with total station under current station, and the target points with the laser tracker. If the measurement task is not finished, move the laser tracker to the next station and repeat the step 3; otherwise, proceed with step 4;
4. Solve the measurement data using the length–angle mixed intersection adjustment model;
5. Evaluate the accuracy of the distance between target points after adjustment.

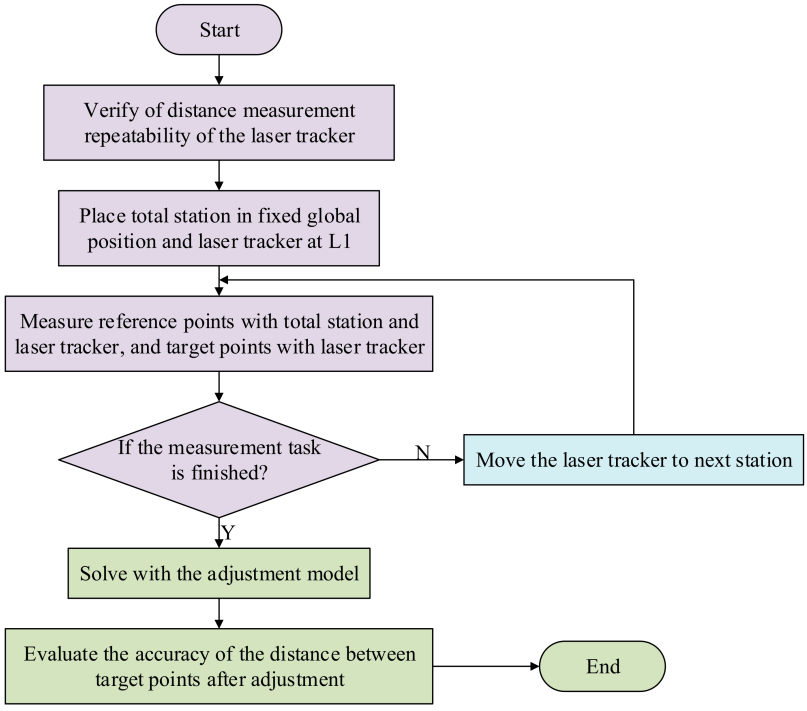


Figure 13. Flow chart of the experimental process.

The equipment used in the experiment included a Leica MS60 total station and a Leica AT402 laser tracker. The laser tracker is moved along a track approximately 669 m in length, adopting a station-transfer method. As shown in Figure 14, the laser tracker measured both target points and reference points, undergoing 10 station transfers, with 11 laser tracker station positions labeled L1–L11 spaced approximately 60 m apart. The total station, T1, is positioned in the middle of this track segment to measure reference points. The distance between adjacent target points is about 3 m, and reference points are placed around the track to ensure that each laser tracker station can observe a sufficient number of reference points.

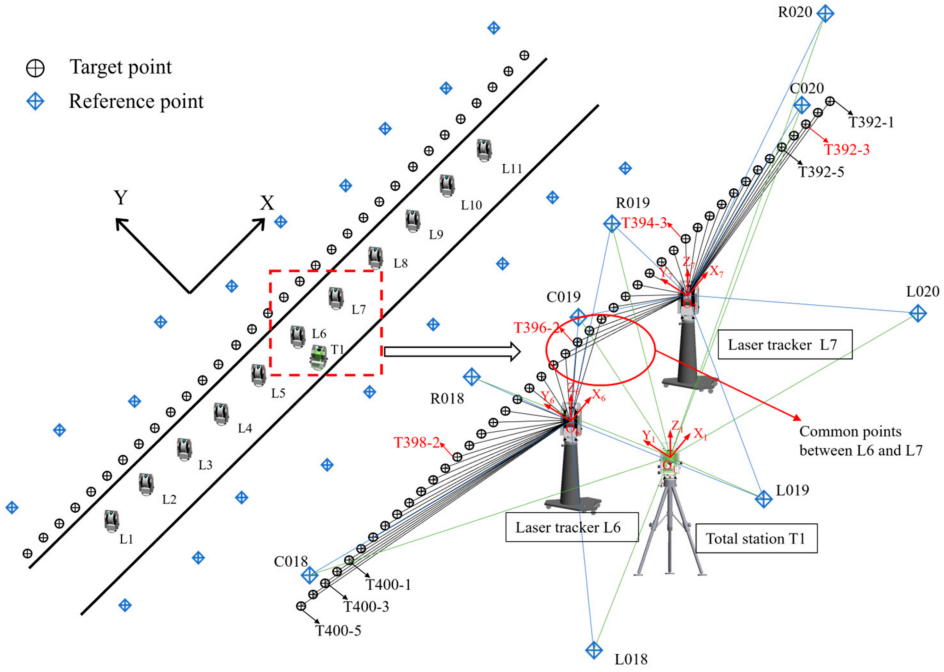


Figure 14. Distribution of measuring stations and points at the experimental site.

The observations of all target points and reference points along the specified track segment are listed in Table 1, which shows the number of measurement points observed by each station.

Table 1. Number of different types of measurement points observed by each station.

Point Type/Station Number	T1	L1	L2	L3	L4	L5	L6	L7~L10	L11
Target points	-	25	25	25	25	25	27	25	25
Reference points	38	7	6	5	6	6	6	6	5

Constructing the error equation according to Formula (13), the number of measurement points and stations is, respectively, as follows:

- n_1 is the number of target points: 224;
- n_2 is the number of reference points: 38;
- m_1 is the number of laser trackers: 11;
- m_2 is the number of total stations: 1;
- The number of unknown parameters is 819;
- The number of equations is 972;
- The number of redundant observation equations is 153.

Substituting these parameters into Formula (16), we can obtain a solution of equations.

4.2. Results and Discussion

Since the true values of the coordinates of the target points to be measured are unknown, the standard deviation of the distance among the target points is used to provide a preliminary evaluation of the accuracy of the measurement control network. By verifying the repeatability precision of the laser tracker within a range of 36 m, the distance standard deviation can be 0.01 mm. According to the principle of slight error, its accuracy can be used to evaluate the distance measurement accuracy of the method proposed in this article. In addition, due to the large amount of data, partial measurement results of target points on the rocket sled test track and distance benchmark measurements by the tracker are listed in Table 2.

Table 2. Coordinates of partial target points after length–angle mixed intersection adjustment.

Name of Target Points	Adjustment Value (mm)				Benchmark Value (mm)			
	X	Y	Z	D	X	Y	Z	D
T418-5	301,016.547	20,846.382	−154.961	30,010.979	6426.496	3452.905	−732.106	30,010.661
T416-5	271,071.847	18,853.947	−217.947		−21,833.926	−6645.488	−835.862	
T414-5	241,130.805	16,861.628	−276.460	30,002.745	6181.262	3590.414	−692.563	30,002.643
T412-5	211,194.338	14,869.440	−338.217		−21,791.810	−7254.398	−929.060	
T410-5	181,269.500	12,880.078	−399.741	30,005.117	6843.273	3449.235	−609.452	30,005.140
T408-5	151,330.618	10,888.560	−464.993		−21,593.847	−6113.811	−1041.582	
T406-5	121,396.550	8893.324	−532.379	29,994.356	−4569.916	6259.200	−817.399	29,994.415
T404-5	91,468.443	6901.757	−591.386		9512.524	−20,223.405	−670.919	
T404-3	85,497.167	6507.226	−613.216	30,009.820	−13,732.183	28,514.641	−818.526	30,008.839
T402-3	55,553.523	4516.372	−676.373		−1661.013	1040.738	−774.919	
T398-2	−7328.702	329.941	−800.793	29,985.668	−357.283	−1720.123	−805.317	29,985.633
T396-2	−37,248.397	−1657.261	−856.687		13,758.912	−28,173.747	−1082.889	
T394-3	−64,192.461	−3447.315	−914.768	29,997.382	−1757.713	866.526	−799.698	29,997.352
T392-3	−94,123.554	−5439.251	−983.907		12,933.449	−25,284.950	−466.316	
T392-5	−88,140.887	−5043.801	−963.617	29,990.500	−17,740.769	33,166.369	−1024.181	29,991.353
T390-5	−118,065.474	−7030.229	−1020.486		−4385.788	6313.378	−817.876	
T388-4	−151,000.444	−9223.686	−1092.545	29,988.119	−16,580.294	30,395.307	−563.565	29,988.103
T386-4	−180,922.572	−11,211.152	−1151.979		−3075.350	3620.855	−741.155	
T382-3	−243,787.618	−15,394.827	−1269.284	29,990.495	−1685.912	1066.893	−772.814	29,990.542
T380-3	−273,711.745	−17,388.306	−1319.127		10,753.667	−26,221.811	−899.742	
T380-1	−279,692.691	−17,785.630	−1326.242	30,029.829	−13,437.210	21,848.443	−869.462	30,029.856
T378-1	−309,656.296	−19,778.164	−1379.070		1176.252	−4385.558	−742.416	

The distance benchmark values compared to the adjusted distances of the target points are shown in Figure 15. We can see that the maximum absolute distance deviation of the target point measured by our method is 0.98 mm, ranging from −0.85 mm to 0.98 mm. The average absolute distance deviation is 0.10 mm, and the standard deviation of distance deviation is 0.20 mm.

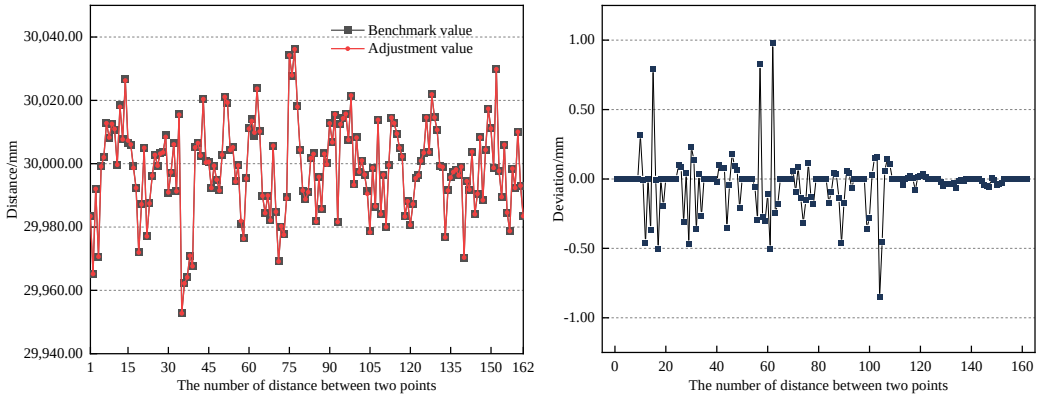


Figure 15. Comparative analysis of distance measurement: (**a**) distance benchmark value and adjusted distance value and (**b**) deviation.

5. Conclusions

The subject of this article is to study a high-precision measurement method for target point coordinates on long straight tracks, such as rocket sled test tracks, and a multi-level measurement strategy based on length–angle mixed intersection adjustment model is innovatively proposed. Initially, based on the analysis of the measurement task and characteristics of the measurement equipment, the measurement control network is divided into multiple levels: Level I includes distances between every two target points, Level II measures coordinates within a small range using laser trackers at different stations, and Level III uses a total station for global data. The length–angle mixed intersection adjustment model is used for data fusion between Level II and Level III, fully utilizing the high-precision distance information from the laser tracker and the high-precision angular information from the total station to control measurement errors. Additionally, to further enhance measurement precision, the simulation analysis of the measurement equipment layout is conducted, providing practical guidance for station placement. Finally, the methods researched are applied in a rocket sled test on a straight track approximately 669 m long, with 224 target points. After solving with the adjustment model, the distances of the target points are compared with the benchmark distances measured by the laser tracker. The deviation range was ± 1 mm, the average absolute value of the deviation was 0.10 mm, and the standard deviation of the deviation was 0.20 mm. The method proposed in this article has significant reference value for the construction of straight track measurement networks and can be applied in various engineering projects such as large-scale generator station construction, tunnel construction, and oil and gas pipeline construction. Moreover, the length–angle mixed intersection adjustment model is also applicable to measurement networks constructed by other distance or angle measuring instruments.

Additionally, uncertainty is crucial for the assessment of the accuracy of three-dimensio nal coordinates. The uncertainty sources of the length–angle mixed intersection adjustment model proposed in this article mainly include distance and angle measurement accuracy, target point run-out, measurement method, Taylor series expansion, etc. In future work, the study of uncertainty will be one of our important research topics.

Author Contributions: Conceptualization, Z.X. and C.L.; methodology, C.L. and Z.X.; software, H.Z., C.Z. and C.L.; validation, Z.X., C.L. and Z.Z. (Ziyue Zhao); formal analysis, Z.X. and C.L.; investigation, C.Z.; resources, Z.X., H.Z. and C.L.; data curation, Z.Z. (Zhongsheng Zhai) and C.Z.; writing—original draft preparation, Z.X. and C.L.; writing—review and editing, Z.X. and C.L.; visualization, H.Z.; supervision, Z.X. and Z.Z. (Ziyue Zhao); project administration, Z.X. and Z.Z. (Zhongsheng Zhai); funding acquisition, Z.X. All authors have read and agreed to the published version of the manuscript.

Funding: The Key Technology of Six-degree-of-freedom Laser Automatic Precise Tracking and Measurement (2019YFB2006100).

Institutional Review Board Statement: Not applicable.

Informed Consent Statement: Not applicable.

Data Availability Statement: Data will be provided by the authors upon request.

Conflicts of Interest: The authors declare no conflicts of interest.

References

1. Vikas; Sahu, R.K. A review on application of laser tracker in precision positioning metrology of particle accelerators. *Precis. Eng.* **2021**, *71*, 232–249.
2. Muralikrishnan, B.; Phillips, S.; Sawyer, D. Laser trackers for large-scale dimensional metrology: A review. *Precis. Eng.* **2016**, *44*, 13–28. [CrossRef]
3. Gao, W.; Kim, S.W.; Bosse, H.; Haitjema, H.; Chen, Y.; Lu, X.; Knapp, W.; Weckenmann, A.; Estler, W.; Kunzmann, H. Measurement technologies for precision positioning. *CIRP Ann. Manuf. Technol.* **2015**, *64*, 773–796. [CrossRef]
4. Xue, B.; Zhu, J.; Zhao, Z.; Wu, J.; Liu, Z.; Wang, Q. Validation and mathematical model of workspace Measuring and Positioning System as an integrated metrology system for improving industrial robot positioning. *Proc. Inst. Mech. Eng. Part B J. Eng. Manuf.* **2014**, *228*, 422–440.
5. Zhang, C.; Jing, X.; Chen, S.; Ling, X.; Zou, J.; Zhao, G. Method of improving large-scale measurement accuracy of laser tracker based on photogrammetry. *Meas. Control* **2019**, *52*, 1220–1227. [CrossRef]
6. Yang, L.H.; Pan, Y.L.; Lin, J.R.; Liu, Y.; Shang, Y.; Yang, S.; Cao, H. Automatic Guidance Method for Laser Tracker Based on Rotary-Laser Scanning Angle Measurement. *Sensors* **2020**, *20*, 4168. [CrossRef] [PubMed]
7. Calkins, J.M. Quantifying Coordinate Uncertainty Fields in Coupled Spatial Measurement Systems. 2002. Available online: https://www.semanticscholar.org/paper/Quantifying-Coordinate-Uncertainty-Fields-in-Calkins/8f4ff9c8a700ea82247de9ba018d19a671f9dc13#citing-papers (accessed on 4 June 2024).
8. Muelaner, J.E.; Wang, Z.; Martin, O.; Jamshidi, J.; Maropoulos, P.G. Estimation of uncertainty in three-dimensional coordinate measurement by comparison with calibrated points. *Meas. Sci. Technol.* **2010**, *21*, 025106. [CrossRef]
9. Manwiller, P.E. Three-Dimensional Network Adjustment of Laser Tracker Measurements for Large-Scale Metrology Applications. *J. Surv. Eng.* **2021**, *147*, 05020009. [CrossRef]
10. Xing, Y.; Dong, L.; Wang, T.; Liang, J.; Ma, N.; Wang, X.; Yang, Z. High-precision and high-efficiency measurement method of accelerator tunnel control network based on total station angle observation. *Meas. Sci. Technol.* **2024**, *35*, 025902. [CrossRef]
11. Guillory, J.; Truong, D.; Wallerand, J.-P.; Lösler, M.; Eschelbach, C.; Mähler, S.; Klügel, T. Determination of the reference point of a radio telescope using a multilateration-based coordinate measurement prototype. *Precis. Eng.* **2023**, *83*, 69–81. [CrossRef]
12. Zhou, Z.; Liu, W.; Wu, Q.; Wang, Y.; Yu, B.; Yue, Y.; Zhang, J. A Combined Measurement Method for Large-Size Aerospace Components. *Sensors* **2020**, *20*, 4843. [CrossRef] [PubMed]
13. Aguado, S.; Santolaria, J.; Samper, D.; Aguilar, J.J. Forecasting method in multilateration accuracy based on laser tracker measurement. *Meas. Sci. Technol.* **2017**, *28*, 025011. [CrossRef]
14. Yang, D.; Zou, J. Precision Analysis of Flatness Measurement Using Laser Tracker. *Int. J. Precis. Eng. Manuf.* **2022**, *23*, 721–732. [CrossRef]
15. Zhao, G.; Zhang, C.; Jing, X.; Sun, Z.; Zhang, Y.; Luo, M. Station-transfer measurement accuracy improvement of laser tracker based on photogrammetry. *Measurement* **2016**, *94*, 717–725. [CrossRef]
16. Lu, S.; Liang, J.; Men, L.; Dong, L.; Wang, T.; Fan, B.; Wang, X.; He, Z.; Yan, L.; Han, Y.; et al. A laser tracker-based multilateration method for pre-alignment of High Energy Photon Source storage ring. *Nucl. Instrum. Methods Phys. Res. Sect. A Accel. Spectrometers Detect. Assoc. Equip.* **2023**, *1045*, 167533. [CrossRef]

Disclaimer/Publisher's Note: The statements, opinions and data contained in all publications are solely those of the individual author(s) and contributor(s) and not of MDPI and/or the editor(s). MDPI and/or the editor(s) disclaim responsibility for any injury to people or property resulting from any ideas, methods, instructions or products referred to in the content.